

# Entropy evaluation sheds light on ecosystem complexity

Mattia Miotto\* and Lorenzo Monacelli†

*Department of Physics, University “Sapienza”, Piazzale Aldo Moro 5, 00185, Rome, Italy*

(Dated: December 3, 2024)

Preserving biodiversity and ecosystem stability is a challenge that can be pursued through modern statistical mechanics modeling. Environmental changes and human activity threaten the fauna of many geographical areas. We exploit the entropy definition from thermodynamics to assess ecosystem stability. In particular, we study a minimal ecosystem on a lattice in which two species struggle for survival. Entropy is measured both in the Shannon-Fano approximation and through a new least entropy principle, based on Maximum Entropy algorithm, that enables the entropy computation in a variational framework. The comparison between the two entropies allows us to measure the degree of long-range ordering in the system. Furthermore, entropy sheds new light on three different phase transitions the system undergoes by tuning animal phenotypes, two being of second order and one of first order. In the latter, the whole ecosystem transits abruptly into an extinction state, causing an ecological catastrophe very difficult to predict, since no precursors indicate the imminent disaster.

## I. INTRODUCTION

The general formulation of statistical mechanics and information theory opened the way of physics to complex systems. The entropy definition is the basis of both theories. Although the concept of entropy first appeared in thermodynamics, it has been adapted in other fields of study, including economics, biophysics, and ecology.

In this work we focus our attention on an ecological system and its entropy, which we show to be pivotal in understanding how the phenotype, the characteristics of an organism resulting from the interaction between its genotype and the environment [1, 2], discriminates between survival and extinction of species. This is a very important effort that must be pursued in order to prevent ecological disasters.

In a very general way, entropy is a property of the distribution function out of which the states of the system have been drawn. It is the capacity of the data to provide or convey information [3]. Consequently, knowing the entropy allows us to set limits to the information we can extract from observations and to the predictability of the system. It has been widely used to study information transport in neural networks [4, 5] and in flocks of birds [6–8], complexity and hierarchy in written languages [9] and risk analysis in financial markets [10, 11]. In particular, predictability plays a very important role in economics where the awareness of markets entropy allows us to maximize the investment profits [10]. Recently, entropy has been exploited in inference problems, with great results in biological phenomena, such as bacterial growth [12, 13], evolution [14] and protein folding [15].

Here, we show how entropy is crucial also in the context of ecological systems. Ecosystems can be defined as a community of living organisms in conjunction with the

environment [16, 17], where the latter affects the organisms without being in turn influenced by them [18]. On the other hand, all living beings within the ecosystem are interdependent, in fact, variations in the size of one population influence all others. This is particularly clear for prey and predator dynamics. In fact, if the number of preys in an ecosystem grows, predators will respond to the supply of available food by increasing their number. The growth of predator number will reduce preys until the system can no longer sustain the predator population. The process has either to attain an equilibrium or to end in species extinction. In order to avoid extinction, both preys and predators need to optimize their phenotypes: predators must, for example, adapt for improving efficiency in hunting to catch enough food to ensure survival. Prey species, on the other hand, must be proficient in escaping their predators and reproduction; if enough of them are to survive for the species to endure [19–21]. Disturbances, which are perturbations that move the system away from its equilibrium state [22], may affect species phenotypes. Such disturbances can originate from changing of environmental variables such as temperature and precipitation or in modifications of the populations, like the appearance/disappearance of a species. Besides the theoretical challenge of understanding the behavior of that kind of complex systems, worthy of notice is also the practical importance of predicting the response to perturbations, particularly the ones produced by humans. Relevant cases are the fight against parasites in agriculture [23] and the perturbations in sea populations due to fishing activities [24]. From the groundbreaking works of Lotka [25] and Volterra [26] ecosystem modeling has been addressed in various ways, from sets of differential equations [27–29] to simulations on lattice [30–32].

Taking inspiration from the work of Dewdney [33] we modeled the simplest nontrivial ecosystem in which two species struggle for survival. Sharks (predators) and fishes (preys) occupy the nodes of the toroidal 2D lattice; they can move, reproduce and hunt. The rules of the model resemble the ones described by Mobilia et al. [34]

---

\*Electronic address: [mattia.miotto@roma1.infn.it](mailto:mattia.miotto@roma1.infn.it)

†Electronic address: [lorenzo.monacelli@roma1.infn.it](mailto:lorenzo.monacelli@roma1.infn.it)

and are introduced in Sec. II C 1. This system has been extensively studied and several critical behaviors have been observed [35, 36].

Measuring the entropy of this kind of complex system without any explicit expression for a *prior* probability distribution is very challenging [37]. In fact, the Shannon definition of entropy relies on the system probability distribution  $P$ , which depends on all the degrees of freedom of the system [38]. The entropy measurement requires a fine sampling of this function, becoming not affordable even for small lattices.

The Maximum Entropy (MaxEnt) technique has been developed in order to obtain an approximation for the probability distribution. Given a set of observables  $x_i$  that partially describes the inquired system, MaxEnt algorithm allows finding the less structured probability distribution that reproduces the chosen set of the real system observables. This technique was firstly introduced by Jaynes [39] in 1957, but it reached an outstanding interest only recently thanks to the availability of a huge amount of experimental and numerical data. MaxEnt has been successfully applied to countless problems, both in equilibrium and out-of-equilibrium systems [40]; among them, the prediction of protein amino acid contacts [15, 41] and the analysis of neural networks [42] are of particular interest. However, even if MaxEnt enables one to extract an analytic expression for the probability distribution, computing the associated entropy is still a major issue [7].

In sec. II A we outline how it is possible to obtain the exact entropy of the MaxEnt probability distribution taking advantage of all the data generated during the convergence of the algorithm, without any further time-consuming computation. Furthermore, in sec. II B, we introduce a *least* entropy principle that justifies the use of the MaxEnt distribution as a truncation of a series that converges toward the real entropy of the system. Availing the variational principle, the approximation on the resulting entropy is of second order. In sec. II C we apply this method to the ecosystem and in sec. III we examine the insights the entropy provides. Although we apply this method only to the introduced ecosystem, it is very general: it can be used whenever it is possible to define a probability distribution on a site model.

### A. Maximum Entropy algorithm

The MaxEnt framework we are going to discuss can deal with any stochastic process defined on a graph composed by  $M$  nodes. Each node is in one out of  $q$  possible states. If we indicate with  $P$  the probability that the system is in a given configuration the entropy is defined accordingly to Boltzmann-Shannon as:

$$S[P] = -\langle \ln P \rangle_P, \quad (1)$$

where  $\langle \cdot \rangle_P$  indicates the average over the  $P$  probability distribution.

The standard MaxEnt algorithm consists in maximizing  $S[P]$  with respect to  $P$  in presence of a set of  $N$  constraints. The restraints are the set of observables  $\{x_i\}_{i=1}^N$  that best describes the system; in other words, some degrees of freedom are fixed and the entropy is maximized among the remaining ones in order to have the broadest possible probability function. Each observable  $x_i$  is a generic function that associates any possible configuration of the system to a real number. Note that the index  $i$  identifies the observable in the set of constraints, not the specific site on the graph, as the  $x_i$  observable can be a function of more than one node, e.g. the average dimension of clusters of nodes in the same state.

Defining the auxiliary Lagrange constrained functional  $\Phi$  as:

$$\Phi[P, \lambda_1, \dots, \lambda_n] = -S[P] + \sum_{i=1}^N \lambda_i \langle x_i \rangle_P, \quad (2)$$

the correct constrained maximum entropy distribution  $P^*$  is found solving the set of equations:

$$\frac{\delta \Phi}{\delta P^*} = 0 \quad (3a)$$

$$\langle x_i \rangle_{P^*} = \bar{x}_i \quad \forall i = 1, \dots, N \quad (3b)$$

where  $\bar{x}_i$  is the measured expected value of  $x_i$ . Eq. (3) is very hard to solve, even numerically, since  $P$  depends still on  $q^M$  variables.  $P$  can be used to define an auxiliary effective Hamiltonian, according to the Boltzmann definition:

$$P(\vec{\sigma}) = \frac{e^{-H(\vec{\sigma})}}{Z},$$

where  $\vec{\sigma}$  represents the configuration and  $Z$  the partition function that normalizes  $P$ .

Eq. (3a) is solved by the Hamiltonian [39]:

$$H = \sum_{i=1}^N \lambda_i x_i, \quad (4)$$

where  $\lambda_i$  are fixed so that the expectation values of  $x_i$  respect the bounds over the real observables.

The values of  $\lambda_i$  can be obtained analytically only in very few cases. The simplest one is the mean-field solution, where only one-body observables are constrained, e.g. the numbers of nodes in each state. In the latter case the number of observables is equal to the number of states  $q$  and the Lagrange multipliers that satisfy the imposed constraints are:

$$\lambda_i = -\ln \left( \frac{\langle x_i \rangle}{M} \right). \quad (5)$$

The passages to prove Eq. (5) are sketched in appendix A. In this case, the entropy per node is:

$$S' = -\sum_{i=1}^q \left( \frac{\langle x_i \rangle}{M} \right) \ln \left( \frac{\langle x_i \rangle}{M} \right), \quad (6a)$$

$$S = MS'. \quad (6b)$$

This entropy evaluation corresponds to the standard one obtained by the Shannon-Fano algorithm [43, 44]. This is a ‘Hartree-Fock’ theory of the complex system, where the entropy is maximized using topology-independent Hamiltonians only. This framework paves the way to a more precise entropy computation.

## II. RESULTS

The general solution of Eq. (3) has been matter of discussion [42, 45–48]. On the way of Bialek and Ranganathan [48], we introduce an auxiliary function  $\tilde{\chi}^2$  whose global minimum coincides with the solution.

$$\tilde{\chi}^2 = \sum_{i=1}^N W_i (\langle x_i \rangle_H - \bar{x}_i)^2, \quad (7)$$

where  $\langle x_i \rangle_H$  is the average of the  $x_i$  observable computed using the trial Hamiltonian  $H$  while  $\bar{x}_i$  is the average over the real observable evaluated by the data.  $W_i$  are coefficients that do not affect the minimum of the  $\chi^2$ , however, if wisely chosen, may accelerate the convergence process. The  $\tilde{\chi}^2$  function defined in Eq. (7), in the minimum, is a random distributed Pearson variable only if all the observables are independent from each other and the  $W_i$  correspond to the inverses of the variances. This is not true in most MaxEnt applications, e.g. in the mean field case where the sum of the  $x_i$  is fixed to  $M$ .

We propose the introduction of a corrected  $\chi^2$  that takes into account linear correlations.

$$\chi^2 = \sum_{\substack{i=1 \\ j=1}}^N (\hat{x}_i - \langle x_i \rangle_H) (\Sigma^{-1})_{ij} (\hat{x}_j - \langle x_j \rangle_H), \quad (8)$$

where  $\Sigma$  is the covariance matrix between the  $N$  chosen observables. It must be stressed that Eq. (8) is still not a true  $\chi^2$  variable, since we corrected only linear correlations. Moreover, eigenvectors of  $\Sigma$  will be uncorrelated, but not necessarily independent. However, linear approximation for correlations between observables has a long history in statistical analysis [49, 50] and usually leads to very good results.

Eq. (8) is well defined only if  $\Sigma$  can be inverted. Diagonalizing the covariance matrix  $\Sigma$ , we can restrict the minimization only in the subspace spanned by its eigenvectors whose eigenvalues are greater than zero. Using these eigenvectors  $y_i$  as a basis, the Pearson  $\chi^2$  can be redefined as:

$$\chi^2 = \sum_{i=1}^{N'} \frac{(\hat{y}_i - \langle y_i \rangle_H)^2}{\tilde{\sigma}_i^2}, \quad (9a)$$

$$N' = N - \dim \ker \Sigma, \quad (9b)$$

$$y_i = \sum_{j=1}^N S_{ij} x_j, \quad (9c)$$

where  $\tilde{\sigma}_i^2$  is the  $i$ -th eigenvalue of the  $\Sigma$  matrix and  $S$  is a  $N' \times N$  matrix that diagonalizes  $\Sigma$ . The  $\dim \ker \Sigma$  indicates the dimension of the  $\Sigma$  kernel.

The gradient of Eq. (8) can be computed as follows:

$$\frac{\partial \chi^2}{\partial \lambda_k} = -2 \sum_{i=1}^{N'} \frac{(\hat{y}_i - \langle y_i \rangle_H)}{\tilde{\sigma}_i^2} \frac{\partial \langle y_i \rangle_H}{\partial \lambda_k}, \quad (10a)$$

$$\frac{\partial \langle y_i \rangle_H}{\partial \lambda_k} = \sum_{j=1}^N S_{ij} \frac{\partial \langle x_j \rangle}{\partial \lambda_k}, \quad (10b)$$

$$\frac{\partial \langle x_j \rangle}{\partial \lambda_k} = -\sigma_{jk}^{MC}. \quad (10c)$$

where  $\sigma_{jk}^{MC}$  is the covariance matrix between observables  $x_j$  and  $x_k$  for the current Hamiltonian:

$$\sigma_{jk}^{MC} = \langle x_j x_k \rangle_H - \langle x_j \rangle_H \langle x_k \rangle_H. \quad (11)$$

The final expression of the gradient is:

$$\frac{\partial \chi^2}{\partial \lambda_k} = 2 \sum_{i=1}^{N'} \frac{(\hat{y}_i - \langle y_i \rangle_H)}{\tilde{\sigma}_i^2} \sum_{j=1}^N S_{ij} \sigma_{jk}^{MC}, \quad (12)$$

or, equivalently, in a compact form:

$$\vec{\nabla} \chi^2 = 2S^\dagger \sigma'_{MC} \left( \frac{\vec{\Delta} y}{\sigma^2} \right), \quad (13)$$

where  $\sigma'_{MC}$  is the Monte Carlo covariance matrix in the non singular subspace and  $\vec{\Delta} y / \sigma^2$  is the vector:

$$\left( \frac{\vec{\Delta} y}{\sigma^2} \right)_i = \frac{\hat{y}_i - \langle y_i \rangle_H}{\tilde{\sigma}_i^2}. \quad (14)$$

The minimization of Eq. (8) can be initialized by the mean-field solution (5), choosing zero for each  $\lambda_i$  associated with a non topology-independent observable. Eq. (12) ensures that any standard gradient-based minimization algorithm can be used.

Moreover, in order to fasten the convergence[51], it is possible to derive the expression of the Hessian matrix in the minimum and utilize it as a precondition on the minimization:

$$D_{hk} = \left. \frac{\partial^2 \chi^2}{\partial \lambda_k \partial \lambda_h} \right|_{\vec{\nabla} \chi^2 = 0}, \quad (15)$$

$$D_{hk} = 2 \sum_{i=1}^{N'} \frac{1}{\tilde{\sigma}_i^2} \sum_{j=1}^N S_{ij} S_{il} \sigma_{jk}^{MC} \sigma_{hl}^{MC}, \quad (16)$$

or, equivalently:

$$D = 2\sigma_{MC} S^\dagger \Sigma^{-1} S \sigma_{MC}. \quad (17)$$

### A. Entropy evaluation

In usual MaxEnt implementations, minimization data are wasted and information about the system is inferred solely from the final probability distribution. Here we show how to recycle the whole minimization procedure to infer the entropy of the system. In fact, computing the entropy directly from the converged probability distribution is a very challenging task. However, entropy can be obtained from an adiabatic integration through the minimization path of the Hamiltonians. The values of the observables during the minimization can be used to obtain a measurement of the entropy of the system without any further Monte Carlo computation.

To compute entropy, it is convenient to define, as done for the effective Hamiltonian, an auxiliary function that is equivalent to the Helmholtz free energy:

$$F = -\ln Z,$$

which can be computed through a thermodynamic integration along the minimization path. Then, Entropy is obtained by inverse Legendre transformation from the auxiliary free energy of the system. Even if the free energy is not well defined (the energy is defined up to a constant), the entropy is.

The free energy at the final value of the minimization is:

$$F(\xi = 1) = F_0 + \int_0^1 \frac{dF}{d\xi} d\xi, \quad (18)$$

where  $\xi$  is a variable that parametrizes the path of the Hamiltonian during the minimization. The  $F_0$  value is the free energy at the starting condition, that is the non-interacting system.

$$F_0 = -M \ln \left( \sum_{j=1}^q e^{-\beta \lambda_j(0)} \right), \quad (19)$$

---


$$S[\lambda_i(\xi)] = M \ln \left( \sum_{j=1}^q e^{-\lambda_j(0)} \right) + \sum_{i=1}^N \left[ \lambda_i(1) \langle x_i \rangle_1 - \int_0^1 d\xi \frac{d\lambda_i}{d\xi}(\xi) \langle x_i \rangle_\xi \right]. \quad (25)$$


---

The only required quantities are the Hamiltonian during the minimization, i.e. the  $\lambda_i(\xi)$ , and the values of the observables  $\langle x_i \rangle_\xi$ , both already computed during the minimization. In addition, if all the configurations generated during the  $\chi^2$  minimization are stored, the importance sampling (IS) can be used to interpolate between different Monte-Carlo points, providing a very good sampling of the integral. IS implementation for the minimization is discussed in Appendix B.

$$F_\xi = -\ln Z_\xi, \quad (20)$$

$$\frac{dF}{d\xi} = \left\langle \frac{dH_\xi}{d\xi} \right\rangle_\xi. \quad (21)$$

The integral can be done parametrizing the Hamiltonian as:

$$H_\xi = \sum_{i=1}^N \lambda_i(\xi) x_i, \quad (22)$$

where  $x_i$  are the observables while  $\lambda_i$  are both the Lagrangian multipliers of the MaxEnt algorithm and the parameters through which the  $\chi^2$  function is minimized. Therefore we get:

$$\frac{dF}{d\xi} = \sum_{i=1}^N \frac{d\lambda_i}{d\xi} \langle x_i \rangle_\xi, \quad (23)$$

so that only the averages of the observables during the minimization are required in order to compute the free energy:

$$F = \langle H \rangle - TS, \quad (24a)$$

$$S = \frac{\langle H \rangle - F}{T}. \quad (24b)$$

Fixing  $T = 1$ , we obtain:

### B. Least maximum entropy principle

Entropy can be defined in the framework of a least principle. The MaxEnt approach finds the probability distribution that maximizes the entropy on the subset where the expected values of the observables  $x_i$  are constrained. The entropy  $S_{ME}$  associated with the MaxEnt probability distribution is greater than the true entropy  $S_{real}$  of the system since the true  $P$  lies in the chosen

subset.

$$S_{real} \leq S_{ME}. \quad (26)$$

Moreover,  $S_{ME}$  decreases whereas new constraints are added due to a contraction of the probability distribution space. In Appendix C we provide a rigorous proof of the fact that a set of constraints that ensures Eq. (26) to become an equality exists. The true entropy of the system is then the least maximum entropy of all possible choices of the constraints.

Just like any variational least energy principle in physics, from Hartree-Fock to *density functional theory* (DFT), the energy (entropy in our case) and its derivatives are the targets of the theory, while the wave functions (probability distributions) are *side-effects*. We want to remark that the error on the entropy due to the limited number of constraints is of second order, while the resulting probability distribution is affected by a first order error.

### C. Ecosystem analysis

Although the so far introduced method is quite general, we discuss its implication in ecosystems. In particular, we analyze a two dimensional model on a regular lattice, limiting the constraints (see section II B) to the on-site densities (mean-field) and near neighbor pairwise correlations. The corresponding MaxEnt Hamiltonian describes a Potts-like system [52].

#### 1. Model definition

Along the lines of Dewdney [33] and Mabilia et al. [34], we modeled a minimal ecosystem composed of two species interacting each other as a 2D lattice model. Each site can be occupied either by the environment or a fish or a shark, respectively represented with the integers 0,1,2. At every time step, fishes can move, breed or remain still with probability  $p_f^m$ ,  $p_f^f$  and  $1-p_f^m-p_f^f$ . Sharks can move ( $p_s^m$ ) or remain still ( $1-p_s^m$ ). Furthermore, sharks eat fishes whenever they step into a cell occupied by a prey. In this case, sharks can reproduce with probability  $p_s^f$ . If a shark does not eat a fish during its round, it can die with probability  $p_s^d$ . This set of rules defines a Markovian process described by the transition matrix  $\Pi(\vec{\sigma}_i \rightarrow \vec{\sigma}_j)$ . It gives the probability of the system to transit from the  $\vec{\sigma}_i$  to the  $\vec{\sigma}_j$  state, where  $\vec{\sigma}_x$  identifies the values of all sites in the lattice. The probability to find the system in the  $\vec{\sigma}_i$  state at the  $t+1$  time step is defined by:

$$P(\vec{\sigma}_i, t+1) = \sum_{\vec{\sigma}_j} \Pi(\vec{\sigma}_j \rightarrow \vec{\sigma}_i) P(\vec{\sigma}_j, t). \quad (27)$$

Studying the time evolution of  $P(\vec{\sigma}, t)$  through Dynamical Monte Carlo simulations (see appendix D) it is possible to assess that the system reaches an equilibrium

distribution:

$$P(\vec{\sigma}_i) = \sum_{\vec{\sigma}_j} \Pi(\vec{\sigma}_j \rightarrow \vec{\sigma}_i) P(\vec{\sigma}_j). \quad (28)$$

Depending on the choice of the parameters, the system that we named EcoLat (*Ecosystem on Lattice*) presents three different kinds of equilibrium configurations: i) fish saturation due to the extinction of sharks; ii) life extinction, where sharks eat all fishes and then extinguish. iii) Steady-state dynamical equilibrium, in which fish and shark densities fluctuate around a constant value.

The probability distribution can be defined extracting configurations from the evolving system after *thermalization*. Sampling configurations sufficiently distant in time it is possible to introduce an ergodic hypothesis (appendix E), i.e. the so defined probability distribution is equivalent to the one of an infinite ensemble of independent systems. In this framework the entropy becomes a well-defined quantity.

#### 2. MaxEnt distribution benchmark

The configurations extracted from EcoLat are used to evaluate the constraints of the MaxEnt distribution. We found a good agreement between MaxEnt and EcoLat distributions (FIG. 1).

In FIG. 1(a-b) two sample configurations are compared. The general aspect of the system is well reproduced by near neighbors MaxEnt, except the shape of the shoals that exhibits some differences. Indeed, EcoLat shoals of fishes are more roundish and localized. This is confirmed by the spatial correlation function in FIG. 1(c), computed as the Pearson coefficient:

$$f_{ij}(x) = \frac{\langle \sigma_i(X) \sigma_j(X+x) \rangle - \langle \sigma_i(X) \rangle \langle \sigma_j(X+x) \rangle}{\sqrt{(\langle \sigma_i(X)^2 \rangle - \langle \sigma_i(X) \rangle^2)(\langle \sigma_j(X)^2 \rangle - \langle \sigma_j(X) \rangle^2)}}, \quad (29)$$

where  $\sigma_i(X)$  is one if the site  $X$  is occupied by the  $i$ -th species; note that  $f_{ij}$  does not depend on  $X$  thanks to the translational symmetry of the system. MaxEnt approximation, although it maintains qualitative agreement, predicts lower fish spatial correlation. This does not affect the cluster size distribution, see FIG. 1(d), that decays with the same slope both in EcoLat and MaxEnt.

The power-law decay in EcoLat has been already observed [53] and assigned to a self-organized behavior of the system, moreover, it seems to be a general characteristic of several spatial ecology models [54].

The comparison avers that the MaxEnt approach, limited to near-neighbor correlations, provides a quite good approximation of the real system. The MaxEnt distribution is very close to a critical point. This can be checked by introducing a parameter  $T$  in analogy to the Boltzmann temperature, however, the  $T$  dependence alone is not an evidence of the criticality in the original system [55].

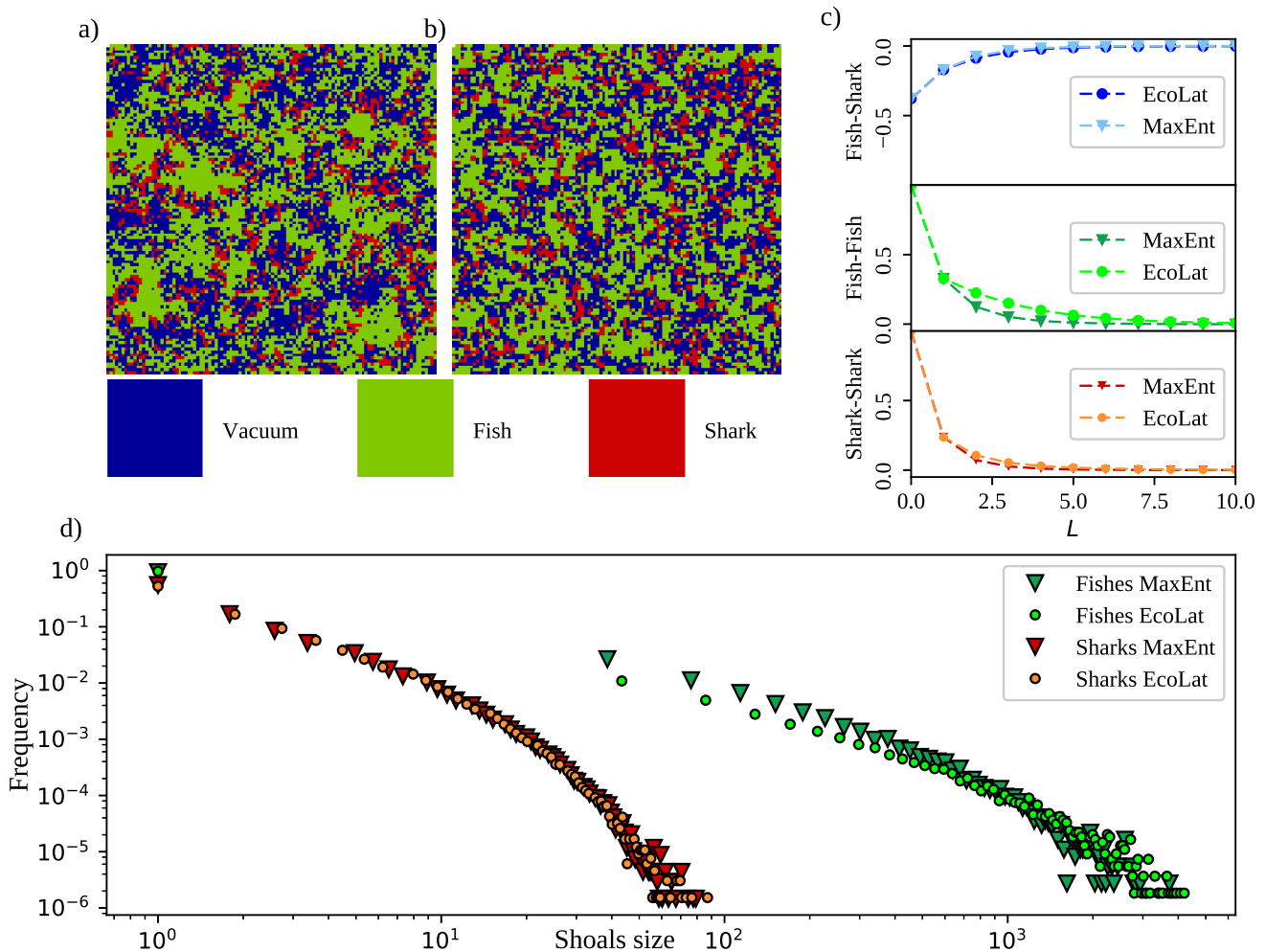


FIG. 1: (Color online) Comparison between the modeled ecosystem (EcoLat) and the Maximum Entropy (MaxEnt) result. **a** Representation of an EcoLat snapshot in the equilibrium regime. Fishes are colored in green, sharks in red, while blue represents the environment. Phenotypic parameters are reported in Appendix F. **b** A configuration extracted from the MaxEnt probability distribution obtained constraining species densities and near neighbor correlations. Both simulations ran on a lattice of edge  $L = 110$ . **c**. Spatial correlation functions of fish-shark (top), fish-fish (medium) and shark-shark (bottom). **d**. Shoal size distribution of fishes (green shades) and sharks (red shades) computed on EcoLat (circles) and MaxEnt (triangles) configurations. Fishes are power-law distributed, while sharks exhibit an exponential decay. The similar power-law exponents in the two distributions indicate that the real system is close to the percolation criticality.

### 3. Entropic curves

Thanks to the method introduced in Eq. (25), it is possible to compute the entropy of the model and to shed light on some not yet grasped features of ecosystems.

In FIG. 2 we report, as a function of the species relevant phenotypes, the entropy per site of the system normalized by its maximal value  $\ln 3$ . The entropy has been measured both through the mean-field Shannon-Fano algorithm (6a) and with the new approach based on the MaxEnt calculation of Eq. (25). The MaxEnt entropy estimation is always lower than the mean-field result, as expected due to the variational nature of the least-entropy-principle. Regions of phenotype values that lead

the system to extinction are filled with obliques lines. FIG. 2(a-b), showing entropy curves as a function of  $p_f^f$  and  $p_s^m$  respectively, manifest qualitative differences between Shannon-Fano and MaxEnt entropy trends. In particular, while Shannon-Fano predicted entropies reach a plateau whenever  $p_f^f \gtrsim 0.5$  or  $p_s^m \gtrsim 0.7$ , MaxEnt ones display a maximum around those values. The increasing difference between Shannon-Fano and MaxEnt entropy is a clear sign that a long-range ordering is occurring. Furthermore, extrapolation of FIG. 2(b-c-d) entropy curves manifests a sharp point in  $p_s^m = 0.4$ ,  $p_f^f = 0.4$  and  $p_s^d = 0.6$ , which are a peculiar sign of a second order phase transition between coexistence and extinction equilibria. On the contrary, when  $p_s^m = 0.9$  or  $p_s^d = 0.1$  en-

ropy displays a sudden jump into the extinction phase, through a first order phase transition.

### III. DISCUSSION

Entropy measurements in complex systems have always been challenging. MaxEnt is a powerful tool to obtain an estimation of the probability distribution of the system from simulations or experimental data. Until now, the information provided by the intermediate steps of the MaxEnt solution was wasted. We introduce a way to recycle it in order to directly evaluate the entropy of the system without any further time-consuming computation (Eq. 25). Thanks to the MaxEnt nature of the probability distribution, a variational principle for entropy evaluation of the real system can be formulated, which ensures that entropy is always greater or equal to its true value. Moreover, Eq. (25) is quite general, allowing to compute entropy where it is possible to formulate a MaxEnt algorithm.

Among many possible applications, the knowledge of entropy in ecological systems plays a pivotal role describing the complexity due to the phenotype variability. In the studied ecosystem, it unveils the existence of three distinct phases, that join in two critical points. Such phases can be inferred by carefully analyzing FIG. 1 and FIG. 2. The first critical point, marking the passage between species coexistence and extinction, lies where the entropy reaches zero (sharp points in FIG. 2(a-b-c) at  $p_s^m = 0.4$ ,  $p_s^f = 0.4$  and  $p_s^d = 0.6$ ). This kind of criticality is well known in literature [35, 36, 56] and it was characterized by its dynamical properties, where predator population decays in time with a power-law. Such critical point divides an absorbing state where the system is crowded by preys from a phase in which sharks start appearing in small shoals swimming in a sea of fishes. The zero entropy of this critical point can be explained in a Shannon-Fano framework, in fact, the predominance of preys unbalances the average numbers of sharks and fishes. This critical point can be attained diminishing the shark hunting ability as well as their fertility or increasing their mortality. The MaxEnt Hamiltonian lets us identify such phase as a ferromagnetic-like state since fishes create percolating clusters.

Moving away from the aforesaid criticality, fish clusters soon acquire a power-law distribution [54] well described by the MaxEnt approximation (FIG. 1), indicating the presence of a second criticality in the ecosystem. This point sets the boundary between two distinct phases of coexistence: one with a predominance of fishes, the other where both preys and predators form shoals of finite size, see FIG. 3(a). This scenario is sketched in FIG. 3(b), where the system path between the two phases in the space of phenotypes is represented by the dashed line. Is it possible to find a path that crosses the first order boundary? Entropic curves in FIG. 2 give the answer. In fact, in case of a first order phase transition, the entropy

is expected to have a discontinuity. Nor the Shannon-Fano neither the MaxEnt curves show such a jump, invalidating this hypothesis for the analyzed paths.

Another phase-transition between coexistence and extinction is reached decreasing the fish fertility, shark mortality or increasing the shark hunting capability. Contrariwise to the first critical point, the entropy does not continuously go to zero in correspondence of the phase transition, but abruptly jumps to zero (FIG. 2). This discontinuity in the entropy resolves in a first order phase transition. It is worth to notice that in this case, as in any first order phase transition, it is possible to continuously tune the phenotype in order to get a steady-state metastable phase even in the extinction region that lives until a sufficiently large stochastic fluctuation causes a brutal extinction. The existence of this first order like phase transition is very worrying; in fact, it is difficult to predict since no precursors are present and can bring to an ecological catastrophe.

The difference between Shannon-Fano and MaxEnt entropy is a measurement of the long-range ordering of the system. In fact, Shannon-Fano is a topology-independent quantity, while MaxEnt considers all possible correlations occurring in a three-state Potts model. This can be understood through an analogy with the Ising model: in the overcritical region,  $T > T_c$  and no external magnetic field, the Shannon-Fano entropy is always at its maximum value since there is an equal number of spin up and spin down. However, the true entropy decreases as  $T \rightarrow T_c$  since ordered spin domains appear. This kind of ordering cannot be measured only by the shoal size distributions since their power-law decay can potentially be just explained in a mean-field framework: the system is close to the percolation critical point, i.e. one species occupies about half of the lattice sites. The increase of long-range ordering occurring in FIG. 2(a-b) can be explained by the formation of large shoals. While this is easy to understand when the fish breeding probability rises, it is unexpected when shark mobility grows, as they spread faster and can potentially break fish shoals.

As a matter of fact, the entropy curves reported in FIG. 2 are a powerful tool to investigate the system from quite different perspectives. They enable the study of entropic-driven phenomena, like entropic forces, of great importance in many biological systems as flocks of birds [7]. In fact, a system that can rearrange the phenotypes of its species will drift into a state that could be realized in more ways. These effective forces are related to the derivative of entropy. Shannon-Fano depicts very well the qualitative nature of the phase-transitions discussed so far and is a very fast measurement. However, it fails to quantitatively describe the entropy derivative the more we get far from the second-order extinction phase transition, requiring a much more sophisticated method, as the one we introduced here. In particular, in a *naive* equilibrium approach, Shannon-Fano would predict an entropic force almost absent close to the first order extinction, see FIG. 2(b). Contrariwise, the near-neighbor

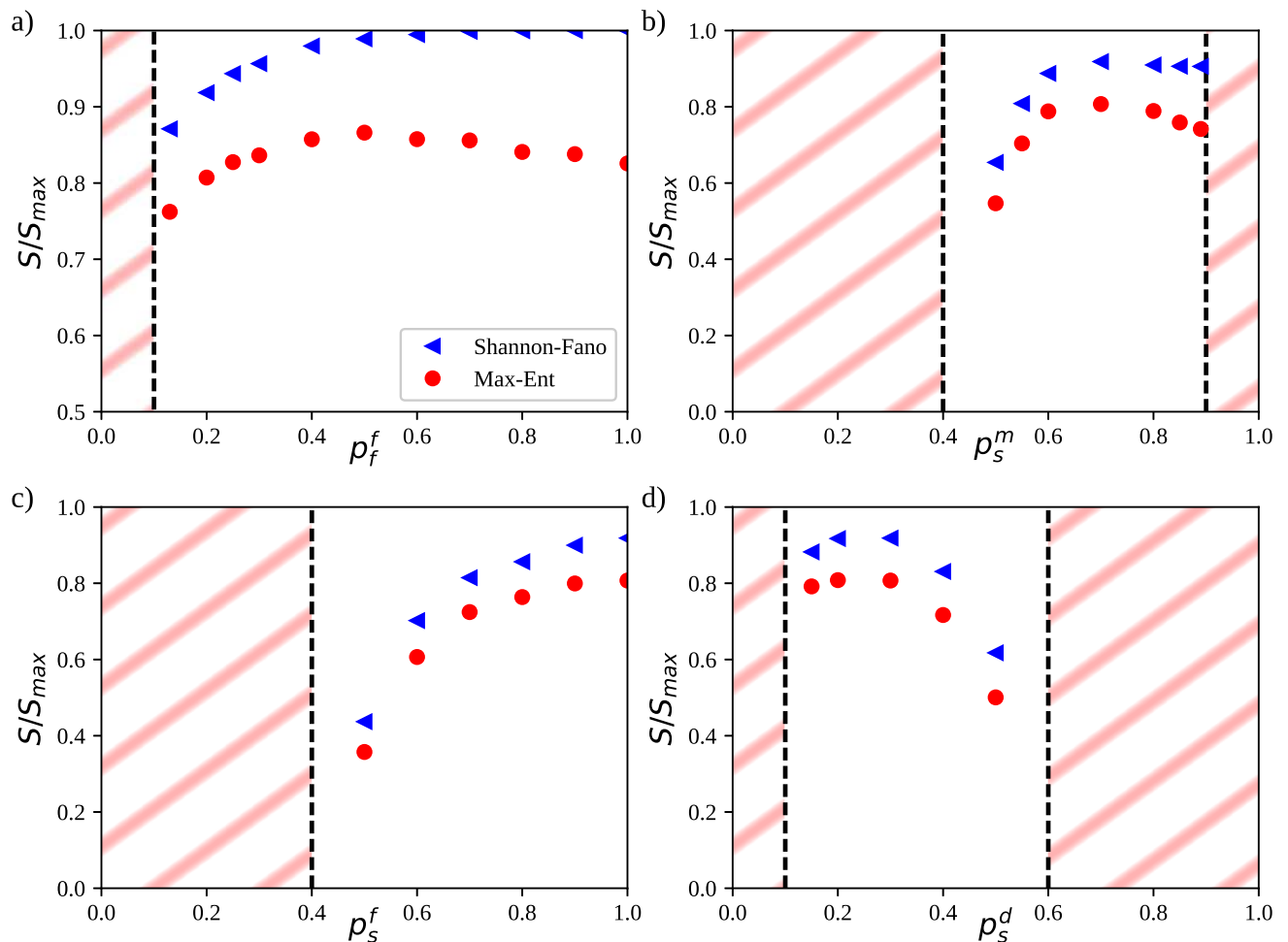


FIG. 2: (Color online) Entropy per site as a function of species phenotypes. Blue triangles indicate the Shannon-Fano entropy (6a) while red circles the MaxEnt entropy (25). The ranges of parameters that lead species to extinction are underlined by oblique lines. **a)** Entropy vs fish breeding probability. A qualitative difference in the entropy behaviors appear when  $p_f^f > 0.5$ ; MaxEnt entropy starts decreasing while Shannon-Fano one saturates to the maximum value. **b)** Entropy vs shark mobility. Also in this case a similar difference in behaviors manifests in the region  $0.7 < p_s^m < 0.9$ . These differences outline that long-range ordering is occurring in the system. **c)** Entropy vs shark filiation. **d)** Entropy vs shark mortality. In these two cases the Shannon-Fano approximation grasps qualitatively well the entropy trends, although the numerical values are overestimated.

correction of entropy predicts a force that helps to preserve the ecosystem.

Overall, we showed how it is possible to shed light on ecosystem stability using the entropy definition from thermodynamics. In particular, the entropy analysis introduced here unveiled three phase transitions, two being of second order and one of first order, that the system undergoes varying the phenotypes of the species. The higher accuracy of MaxEnt entropy estimation over the Shannon-Fano one enables an accurate measurement of long-range ordering in the system and paves the way to get insight of entropic forces in ecological systems. Furthermore, the general nature of the method encourages its application in many other systems of interest.

## Acknowledgments

The authors would like to thank Francesca Tria, Vito D.P. Servedio and Vittorio Loreto for useful insights, Andrea De Martino and Francesco Mauri for helpful discussions.

## Appendix A: Mean-field MaxEnt

Here we derive Eq. (5). In the mean-field approximation, only one body observables  $\{x_i\}_{i=1}^q$  are constrained, e.g.  $\langle x_i \rangle$  is the average number of nodes in the  $i$ -th state. Now, Eq. (4) describes a non-interacting effective Hamil-

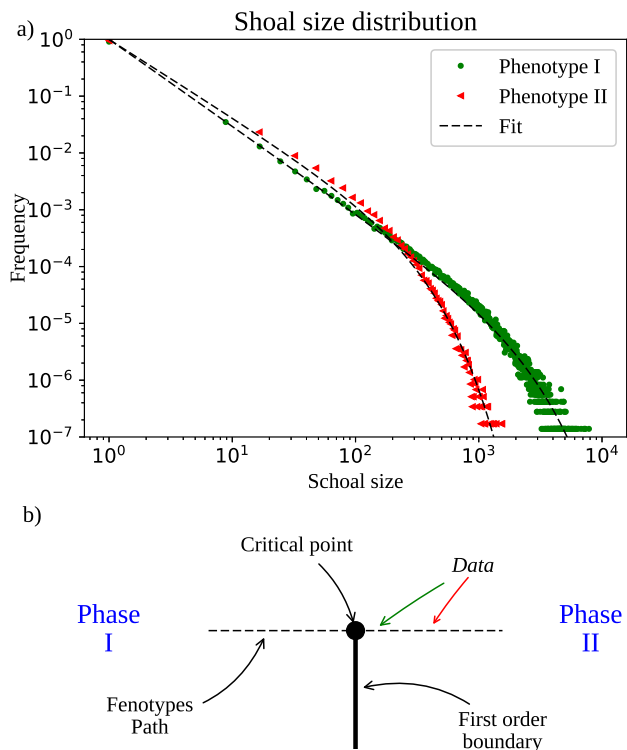


FIG. 3: (Color online) **a** Distributions of prey shoal sizes for two different sets of phenotypic parameters of the ecosystem. The distributions have been fitted with a function  $x^{-\gamma} \exp(x/\xi)$ . “Phenotype I” has  $\xi = 1730 \pm 50$  and  $\gamma = 1.53 \pm 0.01$ , while “Phenotype II” has  $\xi = 211 \pm 8$  and  $\gamma = 1.37 \pm 0.02$ . The fits argue that the two phenotypic realizations have an exponential cutoff that differs by one order of magnitude, confirming the different proximity to a critical point. **b** Sketch of the possible phase diagram associated with this criticality. Changing the phenotypes the system passes from a “Phase I” characterized by percolating clusters of fishes to a “Phase II” in which preys aggregate in finite size shoals. The two data reported in panel (a) are represented by green (left) and red (right) arrows. If the path traverses the first order boundary below the critical point the phase transition is of first order; if it lies above, the system continuously change its phase in an overcritical region; if it crosses the critical point a second order phase transition takes place.

tonian.

$$\langle x_i \rangle = \frac{1}{Z} \sum_{\sigma_1 \dots \sigma_M} \left( \sum_{k=1}^M \delta_{\sigma_k, i} \right) \exp \left( - \sum_{h=1}^q \lambda_h \sum_{k=1}^M \delta_{\sigma_k, h} \right), \quad (\text{A1})$$

where  $Z$  is the normalization of the probability distribution and we identified the configuration  $\vec{\sigma}$  with its site values:

$$\vec{\sigma} = \begin{pmatrix} \sigma_1 \\ \sigma_2 \\ \vdots \\ \sigma_M \end{pmatrix}. \quad (\text{A2})$$

The  $\left( \sum_{k=1}^M \delta_{\sigma_k, i} \right)$  is the application of the  $x_i$  observable on the  $\vec{\sigma}$  state. Since  $x_i$  does not depend on the particular site  $k$  we have:

$$\langle x_i \rangle = M \frac{e^{-\lambda_i}}{\sum_{h=1}^q e^{-\lambda_h}}. \quad (\text{A3})$$

Eq. (A3) defines a complete set of linear equations. They are dependent since we have the constraint:

$$\sum_{i=1}^q \langle x_i \rangle = M \quad (\text{A4})$$

It is straightforward to show that the most general solution of the system is given by:

$$\lambda_i = -\log \left( \frac{\langle x_i \rangle}{M} \right) + C \quad (\text{A5})$$

where  $C$  is an arbitrary constant that does not affect any physical quantity. For sake of simplicity, in Eq. (5) we set  $C = 0$ .

## Appendix B: Importance sampling

The minimization of Eq. (8) is computationally expensive. In each step the expected values of the observables for the trial set of  $\lambda_i$  parameters must be computed through a Monte Carlo-Metropolis integration. A natural extension of the Metropolis algorithm consists into re-weighting the extracted configurations at each step. This method takes the name of Importance Sampling (IS) and it has been widely applied in many physical applications [57, 58]. It was introduced in MaxEnt by Broderick et al. [59].

The average of an observable with an Hamiltonian  $H'$  can be computed using a set uniform distributed configurations  $\{c\}_{i=1}^{N_c}$  as follows:

$$\langle A \rangle_{H'} = \sum_{i=1}^{N_c} \left( A(c_i) \frac{P_{H'}(c_i)}{P_H(c_i)} \right) P_H(c_i) = \langle A \frac{P_{H'}}{P_H} \rangle_H. \quad (\text{B1})$$

This average can be computed using Monte Carlo integration on a set of Metropolis extracted configurations  $\{c'\}_{i=1}^{N_c}$  with the  $H$  Hamiltonian:

$$\langle A \rangle_{H'} \approx \frac{1}{Z(N_c)} \sum_{i=1}^{N_c} A(c'_i) e^{-\beta[H'(c'_i) - H(c'_i)]}, \quad (\text{B2a})$$

$$Z(N_c) = \sum_{i=1}^{N_c} e^{-\beta[H'(c'_i) - H(c'_i)]}. \quad (\text{B2b})$$

Handling with large lattices, energy differences can be considerable, and the exponential term may give rise to numerical instabilities. To correct these instabilities a constant factor  $a$  can be added to both exponential terms,

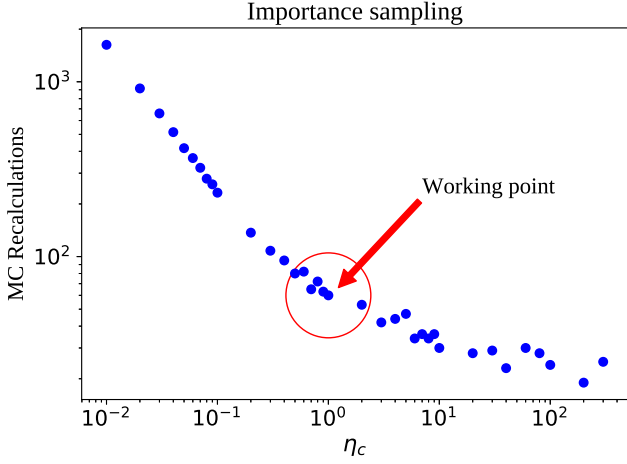


FIG. 4: (Color online) Number of Monte Carlo simulations to reach convergence as a function of the  $\eta_c$  parameter (B3). The optimal working point lies in the marked region.

equal to the maximum energy difference of all extracted configurations.

Estimating the goodness of IS in MaxEnt implementation can be difficult. In fact, we lack the *a priori* knowledge of the partition function of the original probability distribution. In order to upstage, the problem we implemented a new statistical evaluator for the MaxEnt algorithm and in general for IS Metropolis implementation. At each step the total extracted configurations are divided into two random groups and the normalization factors are compared:

$$\eta = \left| \frac{Z'(N_c/2)}{Z''(N_c/2)} - 1 \right|. \quad (\text{B3})$$

If  $\eta$  exceeds a critical value  $\eta_c$ , new configurations are extracted from the Metropolis algorithm. FIG. 4 shows the performance of IS vs the  $\eta_c$  parameter. For  $\eta_c \ll 1$ , Eq. (B3) is symmetric with respect to  $Z'$  and  $Z''$ . For higher values of  $\eta_c$  the symmetry is recovered by random shuffling the configurations at each step.

### Appendix C: Proof of the least maximum entropy principle

By definition, the MaxEnt entropy is always greater than the true entropy:

$$S_{real} \leq S_{ME}[\{\hat{x}_i\}] \quad (\text{C1})$$

where  $S_{real}$  is the real entropy of the system, while  $S_{ME}[\{x_i\}]$  is the maximum entropy of all possible probability distributions that fix the set of  $\hat{x}_i$  observables.

To prove the least maximum entropy principle, a set of observables  $\hat{x}_i$  must exist so that Eq. (C1) is an equality. In any finite size system, where configurations can be

represented with a finite dimension vector, this is trivial, since it is possible to choose a set of observables  $\hat{y}_i$  defined as:

$$\hat{y}_i(\vec{\sigma}) = \delta(\vec{\sigma}, \vec{\sigma}_i), \quad (\text{C2})$$

where  $\vec{\sigma}$  is the configuration on which the observables act,  $\vec{\sigma}_i$  is a particular configuration associated with the observable  $\hat{y}_i$  and  $\delta$  is the Kronecker symbol.

If two probability distributions are different, then a configuration  $\vec{\sigma}_i$  must exist so that their probabilities differ:

$$p_1(\vec{\sigma}_i) \neq p_2(\vec{\sigma}_i). \quad (\text{C3})$$

The two distributions give two distinct expected values for the corresponding  $\hat{y}_i$  observable:

$$\langle y_i \rangle_{p_1} = \sum_j p_1(\vec{\sigma}_j) \delta(\vec{\sigma}_j, \vec{\sigma}_i) = p_1(\vec{\sigma}_i) \neq p_2(\vec{\sigma}_i) = \langle y_i \rangle_{p_2}. \quad (\text{C4})$$

The complete set of  $\hat{y}_i$  fixes the probability distribution, so that

$$S_{real} = S_{ME}[\{\hat{y}_i\}]. \quad (\text{C5})$$

Indeed, single-site density and couple density can be written as linear combination of the complete set of  $\hat{y}_i$  observables. Therefore, the introduction of more independent constraints assures the convergence of the MaxEnt entropy toward the real entropy.

### Appendix D: Dynamical Monte Carlo simulations of the EcoLat model

Dynamical Monte Carlo allows us to simulate the EcoLat master equation (Eq. 27). Since the number of possible states is huge ( $3^M$ ) it is impossible to numerically evolve the probability distribution. However, a stochastic solution of Eq. (27) is still possible:  $N$  replicas of the system, extracted according to an initial distribution  $P(\vec{\sigma}, 0)$ , can be evolved according to the transition matrix  $\Pi$ . The obtained time-dependent ensemble can be used to compute the averages of any observable as a function of time.

The EcoLat model thermalizes, i.e. it reaches the asymptotic equilibrium distribution described by Eq. (28). FIG. 5 shows the time dependence of the mean density of preys and predators as well as the near-neighbor correlation coefficients (Eq. 29).

Note that, although the time evolution of the single system continues to oscillate even at equilibrium, the correlation time is finite. This assures that, after a transient time, all the  $N$  simulations are independent and distributed according to the equilibrium  $P(\vec{\sigma})$  (Eq. 28).

### Appendix E: Ergodic hypothesis

Here we discuss the stability of the equilibrium distribution that depends on the ergodicity of the system [60].

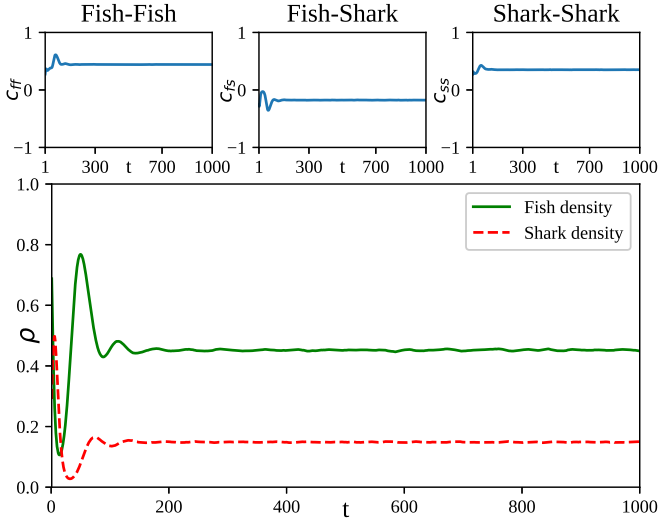


FIG. 5: Time evolution of the mean fish and shark densities and near-neighbour Pearson correlation coefficients computed on an ensemble composed by 100 replicas of the system. The simulation is prepared in an initial uniform distribution fixing the densities of preys and predators to  $4/5$  and  $1/5$  respectively.

Generally speaking, a system is ergodic if it can move between any couple of points in the phase-space in a finite number of steps [61]. EcoLat does not satisfy this requirement, in fact, two traps are present in the phase-space: if the system gets a configuration without preys or predators, it always evolves toward an absorbing state. However, in simulations, once the system has reached the non-absorbing “equilibrium” (FIG. 5), it remains there during all the simulation time. So, we can postulate a weak ergodic hypothesis, where we imagine to restrict the feasible phase-space excluding the absorbing traps. This is equivalent to neglecting the elements of the  $\Pi$  transition matrix that lead the system into the absorbing traps. Such an approximation makes sense if the lifetime  $\tau$  of the meta-stable equilibrium is much larger than the typical time scales of the system. All the Dynamical Monte Carlo simulations computed in FIG. 2 have  $\tau \gg t_{max}$ , where  $t_{max}$  is the maximum simulation time ( $10^6$ ). This is no more true close to the discontinuities in the entropic curves (FIG. 2). However, these regions are close to a first-order phase transition, where also usual thermodynamics predicts a meta-stability of the system.

### Appendix F: Simulation details

Phenotypic parameters for the EcoLat simulation of FIG. 1 and FIG. 3 (Phenotype I) are:  $p_f^f = 0.2$ ,  $p_f^m = 0.8$ ,  $p_s^m = 0.7$ ,  $p_s^f = 1$ ,  $p_s^d = 0.3$ . Phenotypic parameters for the EcoLat simulation of FIG. 3 (Phenotype II) are:  $p_f^f = 0.7$ ,  $p_f^m = 0.3$ ,  $p_s^m = 1$ ,  $p_s^f = 0.9$ ,  $p_s^d = 0.2$ .

All simulations and computations were carried out us-

ing authors handmade C and Python scripts. Python packages NumPy [62], SciPy [63] and Matplotlib [64] were utilized during analysis and figure realization.

- 
- [1] W. Johannsen, *The American Naturalist* **45**, 129 (1911).
- [2] F. B. Churchill, *Journal of the History of Biology* **7**, 5 (1974).
- [3] W. Bialek, *Biophysics: Searching for Principles* (Princeton University Press, 2012).
- [4] S. P. Strong, R. Koberle, R. R. de Ruyter van Steveninck, and W. Bialek, *Physical Review Letters* **80**, 197 (1998).
- [5] I. Nemenman, W. Bialek, and R. de Ruyter van Steveninck, *Physical Review E* **69** (2004).
- [6] W. Bialek, A. Cavagna, I. Giardina, T. Mora, E. Silvestri, M. Viale, and A. M. Walczak, *Proceedings of the National Academy of Sciences* **109**, 4786 (2012).
- [7] M. Castellana, W. Bialek, A. Cavagna, and I. Giardina, *Phys. Rev. E* **93** (2016).
- [8] W. Bialek, I. Nemenman, and N. Tishby, *Neural Computation* **13**, 2409 (2001).
- [9] C. E. Shannon, *Bell System Technical Journal* **30**, 50 (1951).
- [10] J. L. Kelly, *Bell System Technical Journal* **35**, 917 (1956).
- [11] G. C. Philippatos and C. J. Wilson, *Applied Economics* **4**, 209 (1972).
- [12] D. De Martino, F. Capuani, and A. De Martino, *Physical Review E* **96** (2017).
- [13] D. De Martino, F. Capuani, and A. De Martino, *Physical Biology* **13** (2016).
- [14] E. Kussell, *Science* **309**, 2075 (2005).
- [15] M. Weigt, R. A. White, H. Szurmant, J. A. Hoch, and T. Hwa, *Proceedings of the National Academy of Sciences* **106**, 67 (2008).
- [16] A. G. Tansley, *Ecology* **16**, 284 (1935).
- [17] W. C. Allee, *Ecological Monographs* **4**, 541 (1934).
- [18] F. S. Chapin, P. A. Matson, and P. M. Vitousek, *Principles of Terrestrial Ecosystem Ecology* (Springer New York, 2011).
- [19] W. Cooper and D. Blumstein, *Escaping From Predators: An Integrative View of Escape Decisions* (Cambridge University Press, 2015).
- [20] B. A. Belgrad and B. D. Griffen, *Proceedings of the Royal Society B: Biological Sciences* **283** (2016).
- [21] R. S. Olson, A. Hintze, F. C. Dyer, D. B. Knoester, and C. Adami, *Journal of The Royal Society Interface* **10** (2013).
- [22] T. W. Swetnam and J. L. Betancourt, *Journal of Climate* **11**, 3128 (1998).
- [23] P. Kindlmann, H. Yasuda, Y. Kajita, S. Sato, and A. F. G. Dixon, *Frontiers in Ecology and Evolution* **3** (2015).
- [24] N. Bax, *ICES Journal of Marine Science* **55**, 997 (1998).
- [25] A. Lotka, *Proc. Natl. Acad. Sci. U.S* (1920).
- [26] V. Volterra, McGraw-Hill (1931).
- [27] E. E. Holmes, M. A. Lewis, J. E. Banks, and R. R. Veit, *Ecology* **75**, 17 (1994).
- [28] K. Kuto and Y. Yamada, *Journal of Differential Equations* **197**, 315 (2004).
- [29] J. D. Ferreira, C. A. T. Salazar, and P. C. Tabares, *Nonlinear Analysis: Real World Applications* **14**, 536 (2013).
- [30] J. E. Satulovsky and T. Tomé, *Physical Review E* **49**, 5073 (1994).
- [31] A. Lipowski, *Physical Review E* **60**, 5179 (1999).
- [32] U. Dobramysl, M. Mobilia, M. Pleimling, and U. C. Täuber, *Journal of Physics A: Mathematical and Theoretical* (2017).
- [33] A. K. Dewdney, *Scientific American* **251**, 14 (1984).
- [34] M. Mobilia, I. T. Georgiev, and U. C. Täuber, *Physical Review E* **73** (2006).
- [35] T. Antal, M. Droz, A. Lipowski, and G. Ódor, *Physical Review E* **64** (2001).
- [36] U. C. Täuber, *Journal of Physics: Conference Series* **319**, 012019 (2011).
- [37] I. Nemenman, F. Shafee, and W. Bialek, in *Advances in neural information processing systems* (2002), pp. 471–478.
- [38] C. E. Shannon, *Bell system technical journal* (1951).
- [39] E. T. Jaynes, *Physical Review* **106**, 620 (1957).
- [40] A. Cavagna, I. Giardina, F. Ginelli, T. Mora, D. Piovani, R. Tavarone, and A. M. Walczak, *Physical Review E* **89** (2014).
- [41] T. Mora, A. M. Walczak, W. Bialek, and C. G. Callan, *Proceedings of the National Academy of Sciences* **107**, 5405 (2010).
- [42] E. Schneidman, M. J. Berry, R. Segev, and W. Bialek, *Nature* **440**, 1007 (2006).
- [43] C. E. Shannon, *Bell System Technical Journal* **27**, 379 (1948).
- [44] R. M. Fano, *The transmission of Information* (Cambridge: Massachusetts Institute of Technology, Research Laboratory of Electronics, 1949).
- [45] S. W. Lockless, *Science* **286**, 295 (1999).
- [46] M. Socolich, S. W. Lockless, W. P. Russ, H. Lee, K. H. Gardner, and R. Ranganathan, *Nature* **437**, 512 (2005).
- [47] W. P. Russ, D. M. Lowery, P. Mishra, M. B. Yaffe, and R. Ranganathan, *Nature* **437**, 579 (2005).
- [48] W. Bialek and R. Ranganathan, *ArXiv e-prints* (2007).
- [49] K. Pearson, *Philosophical Magazine Series 6* **2**, 559 (1901).
- [50] H. Hotelling, *Journal of Educational Psychology* **24**, 417 (1933).
- [51] S. G. Nash, *SIAM Journal on Scientific and Statistical Computing* **6**, 599 (1985).
- [52] R. B. Potts and C. Domb, *Mathematical Proceedings of the Cambridge Philosophical Society* **48**, 106 (1952).
- [53] B. Sutherland and A. Jacobs, *Complex System* **8**, 385 (1994).
- [54] M. Pascual, M. Roy, F. Guichard, and G. Flierl, *Philosophical Transactions of the Royal Society B: Biological Sciences* **357**, 657 (2002).
- [55] I. Mastromatteo and M. Marsili, *Journal of Statistical Mechanics: Theory and Experiment* **2011**, P10012 (2011).
- [56] U. Dobramysl, M. Mobilia, M. Pleimling, and U. C. Täuber, *arXiv preprint arXiv:1708.07055* (2017).
- [57] G. Torrie and J. Valleau, *Journal of Computational Physics* **23**, 187 (1977).
- [58] I. Errea, M. Calandra, and F. Mauri, *Physical Review B* **89** (2014).
- [59] T. Broderick, M. Dudik, G. Tkacik, R. E. Schapire, and W. Bialek, *ArXiv e-prints* (2007), 0712.2437.
- [60] K. Huang, *Statistical Mechanics* (Wiley, 208).
- [61] R. Palmer, *Advances in Physics* **31**, 669 (1982).
- [62] S. van der Walt, S. C. Colbert, and G. Varoquaux, *Computing in Science & Engineering* **13**, 22 (2011).
- [63] E. Jones, T. Oliphant, P. Peterson, et al., *SciPy: Open*

- source scientific tools for Python* (2001). (2007).
- [64] J. D. Hunter, *Computing In Science & Engineering* **9**, 90